Scientific Research Publishing

Modern Research in Catalysis, 2020, 9, 21-34
https://www.scirp.org/journal/mrc
ISSN Online: 2168-4499
ISSN Print: 2168-4480

Hydroxyl Enhanced Structured Pt/Ni$_x$/a-AlOOH Catalyst for Formaldehyde Oxidation at Room Temperature

Shoudian Zhao[1], Qi Zhang[1*], Guobing Zhao[1], Yuhua Zhang[2]

[1]Engineering Research Center of Large Scale Reactor Engineering and Technology, Department of Chemical Engineering, East China University of Science and Technology, Shanghai, China
[2]Shanghai I-Clearsky Environmental Protection Co., Ltd., Shanghai, China
Email: *zhangqi@ecust.edu.cn

How to cite this paper: Zhao, S.D., Zhang, Q., Zhao, G.B. and Zhang, Y.H. (2020) Hydroxyl Enhanced Structured Pt/Ni$_x$/a-AlOOH Catalyst for Formaldehyde Oxidation at Room Temperature. *Modern Research in Catalysis*, **9**, 21-34.
https://doi.org/10.4236/mrc.2020.92002

Received: February 15, 2020
Accepted: April 10, 2020
Published: April 13, 2020

Abstract

Ni promoted structured plate-type Pt/Ni$_x$/a-AlOOH catalysts were developed to enhance the amount of hydroxyl group, therefore improving the catalytic activities for formaldehyde oxidation at room temperature. The analyzation results by XRD and HRTEM indicate that two kinds of materials, AlOOH and NiOOH, are detected on the surface of Pt/Ni$_x$/a-AlOOH. It can be seen from the result of TG that the hydroxyl group on the catalyst surface increased after Ni was loaded. Furtherly, XPS results show that the percentage of hydroxyl groups which can effectively absorb formaldehyde increases from 36.4% to 72.8% by doping Ni. In addition, the content of Pt^0 increased from 27.5% to 45%. The results indicate that optimized $Pt_{1.15}/Ni_{3.1}$/a-AlOOH has the best catalytic activity with the CO_2 conversion is 88% at 25˚C and 100% at 40˚C, while CO_2 conversion over $Pt_{1.2}$/a-AlOOH is 56% at 25˚C and 100% at 100˚C respectively. Hence, the Ni promoted plate-type Pt/a-AlOOH possesses high efficiency and it provides a new idea for catalyst design of formaldehyde oxidation.

Keywords

Structured Catalyst, AlOOH, Formaldehyde, NiOOH

1. Introduction

Formaldehyde (HCHO) is a typical indoor air pollutant, mainly from furniture materials and home building [1] [2]. Long-term exposuring to HCHO can lead to dizziness, headache, fatigue, nausea, memory loss, decreased immunity, and even to death [3] [4] [5]. Therefore, the elimination of HCHO has a vital impact

on human safety and environmental protection.

Catalytic oxidation technology can completely decompose HCHO into H_2O and CO_2. With low reaction temperature, high efficiency, good stability and no secondary pollution, it has become the focus of researchers. In the process of catalytic oxidation of HCHO, the catalytic properties of different catalysts are quite different. Therefore, the key to catalytic oxidation technology is to find catalysts with high efficiency and low cost. At present, the catalysts used for catalytic oxidation of HCHO include noble metal catalysts (such as Pt, Au, Pd, Ag) [6]-[15] and metal oxides (such as MnO_x and Co_3O_4) [16]-[23]. While among these catalysts, Pt has been widely studied for its remarkable activity. Common carriers are materials with large specific surface area, such as TiO_2 [24] [25], Al_2O_3 [26], AlOOH [27] [28], etc. These materials are conducive to the adsorption and diffusion of reactants and products, and can also enhance the interaction between carriers and active components [29] [30].

Hongfang Li [31] *et al.* prepared the Au/CeO_2 catalyst and tested the activity. The catalyst can oxidize HCHO into CO_2 and H_2O at 50˚C. Chun-Chang Ou [32] *et al.* compared the effect of calcination temperatures and h2 reduction pretreatment on the catalyst. It was found that when calcined at 573K and then reduced by 10% H_2/N_2 at 473K, the formaldehyde can be completely converted at 333K by Ag/CeO_2. Ying Chen [33] *et al.* discussed the effect of alkali metal salt on Pt/mno_2 catalyst. According to the research, Na^+ modification was a simple and effective method to improve the performance of formaldehyde oxidation catalyst, and the conversion rate of formaldehyde can reach 100% at 50˚C. Xiucheng Sun *et al.* supported Rh with titanium dioxide, which can absorb oxygen in the air and convert it into reactive oxygen atom, and oxidize HCHO into CO_2 and H_2O, obtaining outstanding catalytic activity [34]. Bing-bing Chen *et al.* used the deposition-precipitation method to load Au onto γ-Al_2O_3 and pointed out that it had good activity due to the presence of hydroxyl groups on the surface [26]. Zhaoxiong Yan *et al.* used AlOOH as the carrier, loading Au onto AlOOH by impregnation method, and prepared catalysts with high oxidation activity to oxide HCHO by controlling the structure of the carrier and the particle size of the active component [35].

Traditional AlOOH can absorb HCHO, but cannot oxide HCHO. Our previous work [36] found that the anodic AlOOH (a-AlOOH) exhibited a high catalytic activity on HCHO oxidation. The excellent catalytic performance could be attributed to the well-developed {031} {200} {002} facets which generated on the a-AlOOH [37] [38] [39]. Besides, there are more active hydroxyl groups on a-AlOOH. More hydroxyl groups on the catalyst can provide more sites for the adsorption of formaldehyde, which is more conducive to the catalytic oxidation of formaldehyde. Therefore, how to further improve the surface hydroxyl of catalyst is a crucial question. In our previous works [35], Fe was loaded on the catalyst to increasing the hydroxyl content. Because it can form FeOOH, which is good for forming more hydroxyl groups. Tengfei Yang *et al.* supported Ni on the

catalyst, indicating that the hydroxyl formed by Ni was conducive to promoting the oxidation of HCHO at the active site [12]. Therefore, in this paper, we try to increase the hydroxyl content by loading Ni on the catalyst in the form of NiOOH.

In this work, Ni was doped on the plate-type Pt/a-AlOOH catalysts to improve the performance for formaldehyde oxidation at room temperature. Firstly, the physicochemical properties of the catalysts were compared by scanning electron microscopy (SEM) and Brunauer-Emmett-Teller (BET). Secondly, the activities of a-AlOOH, Pt/a-AlOOH and Pt/Nix/a-AlOOH catalysts were evaluated for formaldehyde oxidation at room temperature. Finally, the effects of Ni amount enhancing the hydroxyl groups were investigated by X-ray diffraction (XRD), high-resolution transmission electron microscopy (HRTEM), thermogravimetry (TG) and X-ray photoelectron spectroscopy (XPS).

2. Experimental

2.1. Catalyst Preparation

Catalyst support was prepared by anodization of the 200 × 200 × 0.4 mm plate-type aluminum plate (1060) in a 0.4 wt% oxalic acid solution for 10 hours at 20˚C with the current density of 25 A/m^2. Then the catalyst was calcined at 350˚C for 1 hour in muffle, in order to the residual oxalic acid could be decomposed in the pore structure of the anodic alumite film. To increase the BET surface area of the support, immerse the plate in deionized water at 80˚C for 1 - 2 hours, namely Hot Water Treatment (HWT) [29]. After HWT, the plate was naturally dried at room temperature for 6 hours, the resulting plate was denoted as a-AlOOH. The a-AlOOH support was calcined at 250˚C for 4 h and then was immersed in nickel nitrate solution ($Ni(NO_3)_2$), subsequently washed with deionized water and dried in ambient conditions for 12 hours, denoted as Ni_x/a-AlOOH.

Ni_x/a-AlOOH support was immersed into the mixed solution of 0.1 - 0.8 g/L $H_2PtCl_6{\cdot}6H_2O$ under magnetic stirring for 4 h to achieve the nominal weight of Pt equals to 1.2 wt%, then dried in ambient conditions for 12 hours. Then the catalyst was immersed into $NaBH_4$ solution (0.01 mol/L) for 1h. Finally, the catalyst was washed with deionized water and dried in ambient conditions for 12 hours. The obtained catalyst was denoted as Pt/Ni_x/a-AlOOH.

2.2. Characterizations

The surface morphology of catalysts was characterized by a scanning electron microscopy (SEM) (JSM-6360LV, JEOL). The Brunauer-Emmett-Teller (BET) surface area (S_{BET}) determined by a multipoint BET method, and pore structure of catalysts were obtained from nitrogen adsorption data in the relative pressure P/P_0 range of 0.0 - 1.0 measured by using a Micromeritics ASAP 2020-M nitrogen adsorption apparatus (USA). The single-point pore volume (Vp) and pore size distributions (PSD) were determined by using desorption data by the

Barret-Joyner-Halender (BJH) method.

X-ray powder diffraction (XRD) patterns of the different supports and as-prepared samples were recorded on a Rigaku D/MAX 2550 VB/PC X-ray diffractometer (Japan) using copper-anode radiation operated at 30 kV and 40 mA. The data was collected over the 2θ angle ranging from 10˚ to 80˚ with a scan step of 0.02˚. Transmission electron microscope (TEM) was characterized on a JEM-2100HR TEM (JEOL, Japan). Thermal gravimetric analysis (TGA) of the samples was performed on a WRT-3P TG equipment with a humidity controller. To determine the temperatures at which water molecules were lost as samples were heated. Samples (~10 mg) were heated in N_2 flow (40 $cm^3 \cdot min^{-1}$) at a heating rate of 10˚C·min^{-1} from 25˚C to 650˚C. XPS measurements were analyzed on an XSAM-800 apparatus (Kratos, UK), equipped with Al Kα X-ray with 1486.6 eV as the excitation source, and all the binding energies were calibrated respect to the graphite C 1s peak at 284.8 eV.

2.3. Catalytic Activity Evaluation

The catalytic activity evaluation for the catalytic oxidation of HCHO under atmospheric pressure was performed in a fixed-bed quartz flow reactor (i.d = 10 mm) as shown in Figure 1. Air from a compressor flowed into a bubbler filled with HCHO solution (HCHO: 35%) in a water bath maintained at 30˚C and then mixed with the HCHO stream evaporated by heating. The inlet concentration of HCHO was controlled by adjusting the bath temperature and the air flow rate. The feed gas composition was 180 ppm of HCHO. The total flow rate was 220 mL/min, corresponding to a gas hourly space velocity (GHSV) of 15,000 h^{-1}. The plate-type aluminum monolithic catalyst was cut into 2 - 4 mm^2. Then, approximately 0.3 g catalyst mixed with 1 g quartz sands (20 - 40 plate, Yonghua Co., Ltd.) was packed into the quartz tube reactor. The left and right sides of the reactor were filled with quartz fibers. The catalytic activity tests were conducted at the temperature range from 15˚C to 140˚C. The inlet and outlet gas CO_2 were monitored using a gas chromatograph equipped with a flame ionization detector (FID) and methanizer. Before the gas analysis, the CO_2 was quantitatively converted into methane under H_2 present. A PORAPAK-Q column was used to separate the CO_2 and CO gas. The CO_2 was determined by residence time. The temperature of the ionization detector and the column were 120˚C and 90˚C. The HCHO conversion was calculated using the degree of HCHO consumption.

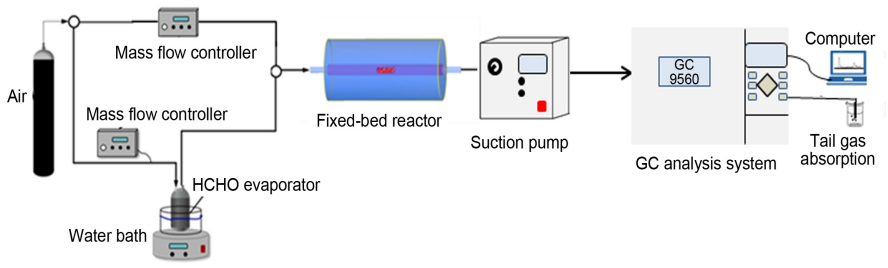

Figure 1. The flow-process chart for catalytic oxidation of HCHO experiment.

The removal percentage of HCHO was calculated as follows:

$$\text{HCHO convers}(\%) = \frac{n_{\text{HCHO},0} - n_{\text{HCHO},0}}{n_{\text{HCHO},0}} \times 100\%$$

where the $n_{\text{HCHO},0}$ and $n_{\text{HCHO,t}}$ represent the concentration of HCHO at the inlet and outlet of the reactor.

3. Results and Discussion

3.1. Structure and Morphology of the Catalyst Support

Figure 2(a) and Figure 2(b) show the surface morphology and structure of a-AlOOH and $Pt_{1.15}/Ni_{3.1}$/a-AlOOH catalyst by SEM. It can be seen that the surface of the catalyst is like honeycomb. The surface of the catalyst changes a little before and after the loading, probably because of the interaction between Pt or Ni and the carrier, indicating that Pt distributed on the surface of the catalyst evenly. This is the same with the specific surface area and pore width in the BET characterization results.

Table 1 shows that with the increasing of Ni content, S_{BET} of the catalyst gradually decreased, but they are all a little bigger than those without Ni, which might be due to the loading of Ni, or because the strong acidity of the $Ni(NO_3)_2$

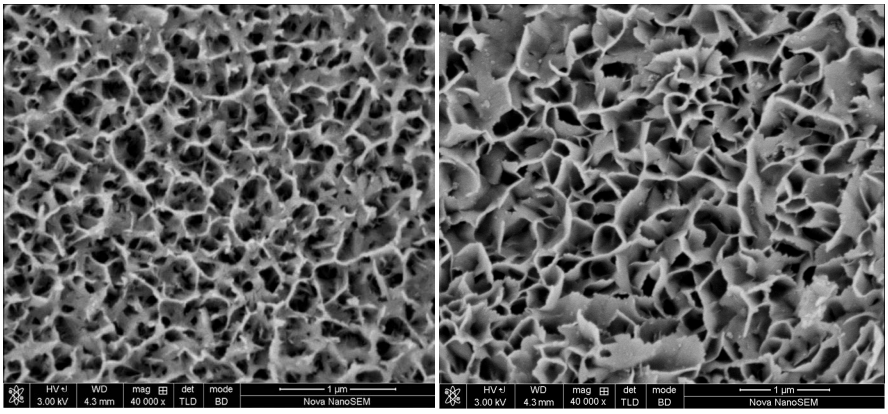

(a) (b)

Figure 2. SEM images of (a) a-AlOOH support (b) $Pt_{1.15}/Ni_{3.1}$/a-AlOOH catalyst.

Table 1. The physical properties of a-AlOOH, $Ni_{3.1}$/a-AlOOH and Pt/Ni_x/a-AlOOH samples.

Catalysts	$S_{BET}/(m^2 \cdot g^{-1})$	$V_{pore}/(cm_3 \cdot g^{-1})$	d_{pore}/nm	Pt/wt%[a]	Ni/wt%[a]
a-AlOOH	86.8	0.13	4.14	N/A	N/A
$Ni_{3.1}$/a-AlOOH	85.0	0.11	4.21	N/A	3.1
$Pt_{1.2}$/a-AlOOH	84.2	0.12	4.20	1.2	N/A
$Pt_{1.10}/Ni_{0.8}$/a-AlOOH	91.0	0.12	4.12	1.10	0.8
$Pt_{1.08}/Ni_{2.2}$/a-AlOOH	92.1	0.10	4.14	1.08	2.2
$Pt_{1.15}/Ni_{3.1}$/a-AlOOH	90.8	0.12	4.10	1.15	3.1
$Pt_{1.05}/Ni_{4.5}$/a-AlOOH	88.6	0.12	4.04	1.05	4.5

Notes: [a]Results of ICP-AES analysis.

(pH = 2.0) corroded the carrier. This may facilitate the formation of surface reacting sites.

3.2. The Promoting Effects of Ni on the Catalytic Activities of Pt/Nix/a-AlOOH

Figure 3 shows the catalytic activities of a-AlOOH, Ni/a-AlOOH Pt/a-AlOOH and Pt/Ni_x/a-AlOOH. Figure 3(a) shows that a-AlOOH can oxidize HCHO at 20˚C with CO_2 conversion of 10%, and 100% at 250˚C. While the HCHO complete oxidation over $Ni_{3.1}$/a-AlOOH is at 120˚C, and the HCHO conversion at 15˚C is 20%, which is higher than that of a-AlOOH. This may be because the presence of Ni in the form of NiOOH enriches the number of surface active hydroxyl groups of the catalyst and provides more active sites.

Meanwhile, Figure 3(b) shows that the catalyst Pt/Ni_x/a-AlOOH has higher oxidation performance than Ni/a-AlOOH and Pt/a-AlOOH. And the catalytic activity of Pt/Ni_x/a-AlOOH increased with the content of Ni before the Ni loading was 3.1 wt%. For the catalyst $Pt_{1.15}/Ni_{3.1}$/a-AlOOH, the HCHO conversion rate was 81% at 15˚C and the complete decomposition temperature of HCHO was 40˚C. While the corresponding for the catalysts Ni/a-AlOOH and Pt/a-AlOOH are 20%, 120˚C and 56%, 80˚C. This may be attributed to the loading of Ni not only enriches the number of surface active hydroxyl groups of

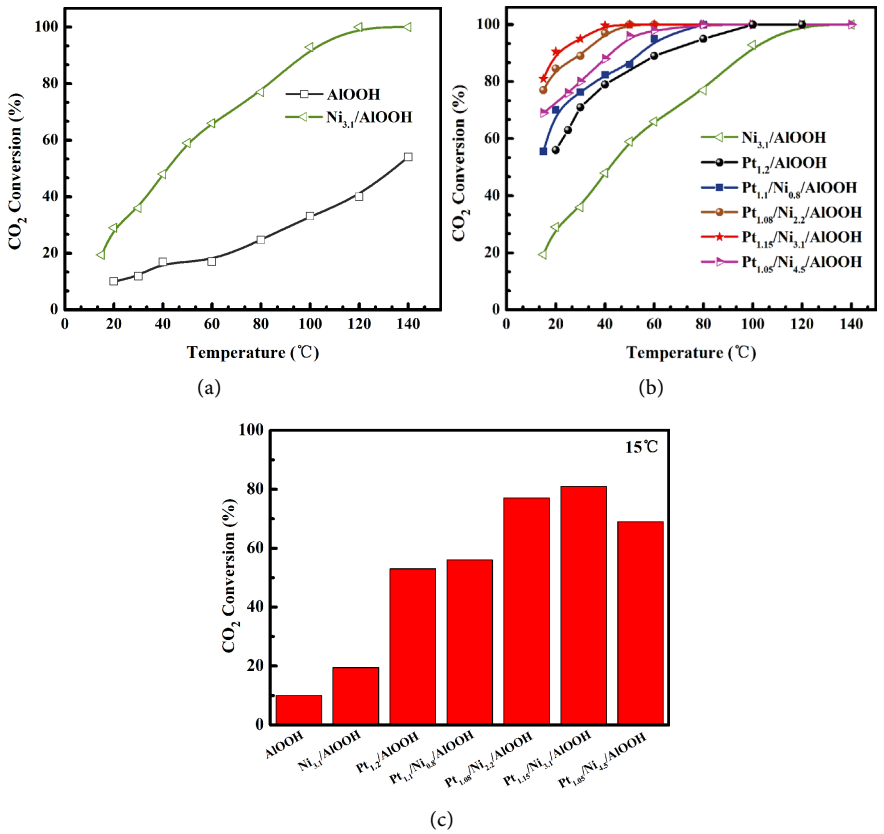

Figure 3. Catalysis performances of Pt/Nix/a-AlOOH catalysts with different Ni loadings, Conditions: X_{HCHO} = 180 ppm, GHSV = 15,000 h^{-1}.

the catalyst, but also increases the content of Pt^0, which is more conducive to converting formaldehyde. Figure 3(c) shows the activities of different catalysts at 15˚C. It can be seen that the catalyst shows the best activity when the Ni content was 3.1 wt%. It can be seen that even at low temperature $Pt_{1.15}/Ni_{3.1}$/a-AlOOH exhibits the activity of 80%, while 55% over $Pt_{1.2}$/a-AlOOH.

Figure 4 displays the XRD patterns of Pt/Nix/a-AlOOH. The diffraction peaks at 14.3˚, 28.2˚, 38.4˚, 49.3˚, 55.2˚, 65.0˚ and 71.7˚ correspond to structured a-AlOOH (a-AlOOH, JCPDS 21-1307) for all catalysts. The diffraction curves of Pt/Ni0.8/a-AlOOH and structured a-AlOOH are similar, which may be because of the low content of Ni and Pt or the small particle size of Ni and Pt. There are diffraction peaks at 12.8˚, 25.9˚ and 37.9˚ and 43.2˚ for $Pt/Ni_{2.2}$/a-AlOOH, $Pt/Ni_{3.1}$/a-AlOOH and $Pt/Ni_{4.5}$/a-AlOOH, which is the characteristic peak of NiOOH (Nickel oxide hydroxide, JCPDS 06-0075), and they correspond {003}, {006}, {101} and {105} faces. Among them, the first diffraction peak of these three samples is obviously different from structured a-AlOOH, possibly because of the influence of Ni diffraction peak. The formation of NiOOH species enables Pt/Nix/a-AlOOH to have two different hydroxyl groups on the surface in addition to water, increasing the content of hydroxyl groups on the surface of the catalyst, thus improving the efficiency of catalytic oxidation of HCHO.

Figure 5 shows the microscopic morphology of $Pt/Ni_{3.1}$/a-AlOOH was observed by TEM and HRTEM. Figure 5(a) shows the microstructure of $Pt/Ni_{3.1}$/a-AlOOH. Some tiny Pt and Ni were loaded on these nanorods, which were attributed to the shape of the plate-like a-AlOOH body after hydration. By further enlarging the magnification, it can be seen that Pt particles have a good dispersion on the catalyst, as shown in Figure 5(b). The black spots in the Figure are Pt particles. It can be seen from Figure 5(b). that Pt particle size distributed between 0.5 and 7.5 nm, while the main particle size is mainly concentrated in the range of 2.75 - 3.75 nm. Combined with XRD testing, the well dispersion of Pt on the catalyst

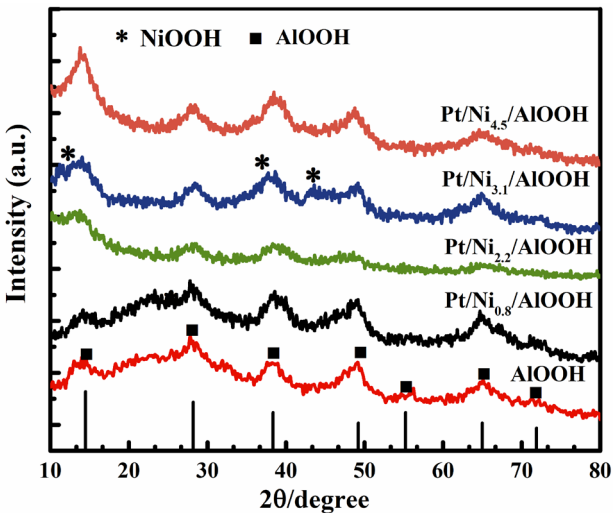

Figure 4. XRD results of a-AlOOH and Pt/Nix/a-AlOOH samples.

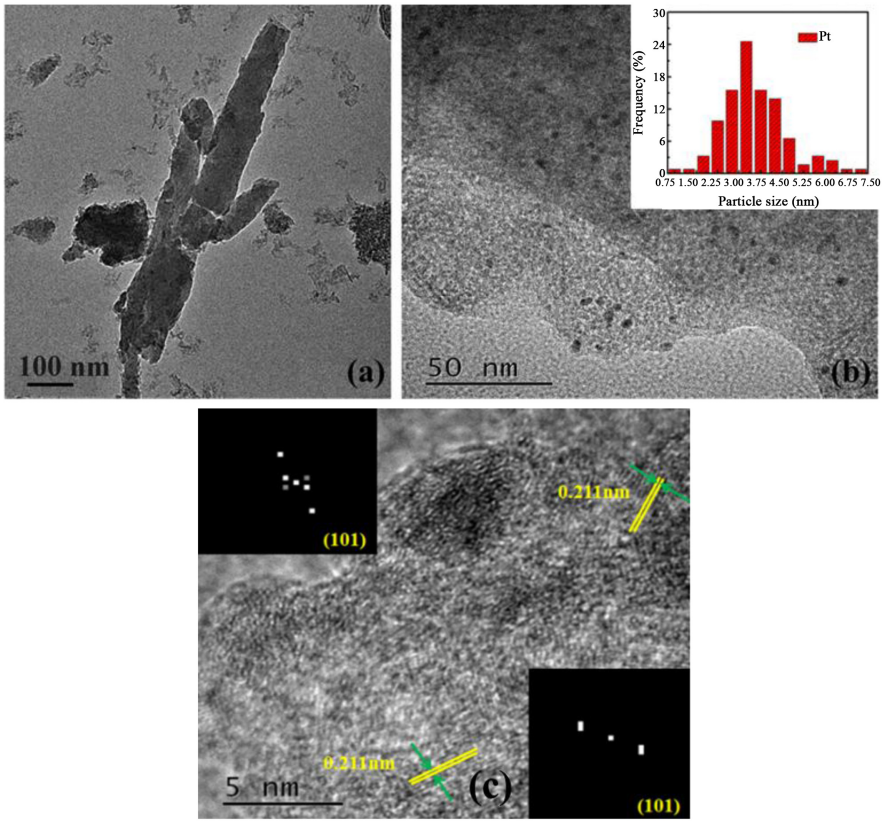

Figure 5. TEM: (a) (b) and HRTEM: (c) images of $Pt_{1.15}/Ni_{3.1}$/A-AlOOH catalyst.

may be due to the impregnation of $Ni(NO_3)_2$, which may be because of abundant surface hydroxyl. Furthermore, HRTEM analysis was carried out to investigate the facets difference of the catalysts, as shown in Figure 5(c). The presence of the $Pt_{1.15}/Ni_{3.1}$/a-AlOOH indicated that the lattice spacing values parallel to the top and om facets are ca. 0.211 which corresponds to the {101} planes of the crystallized NiOOH. The presence of NiOOH increases the content of hydroxyl on the surface of the catalyst, which is conducive to adsorption and conversion of formaldehyde.

Figure 6 shows the influence of the surface composition of a-AlOOH and Pt/Ni3.1/a-AlOOH catalyst on the catalytic performance of the catalysts. The two samples were compared by thermogravimetric (TG) analysis. The region (at ca. 87˚C - 93˚C) for a-AlOOH and the region (at ca. 90˚C - 100˚C) for $Pt/Ni_{3.1}$/a-AlOOH correspond to the weakly physisorbed water molecules, which can be easily removed below 100˚C. The region (ca.260˚C - 460˚C) for a-AlOOH and the region (at ca. 200˚C - 510˚C) for $Pt/Ni_{3.1}$/a-AlOOH are due to the loss of the chemisorbed molecules of structural hydroxyl groups over a-AlOOH, respectively. The overall weight loss of $Pt/Ni_{3.1}$/a-AlOOH was significantly higher than that of a-AlOOH, possibly because of the surface of $Pt/Ni_{3.1}$/a-AlOOH contained two kinds of substance: a-AlOOH and NiOOH. Besides, there is a third weightlessness peak at about 510˚C, which was due to the decomposition Ni_2O_3 into NiO. Because at 300˚C NiOOH may decompose into Ni_2O_3, then Ni_2O_3 was

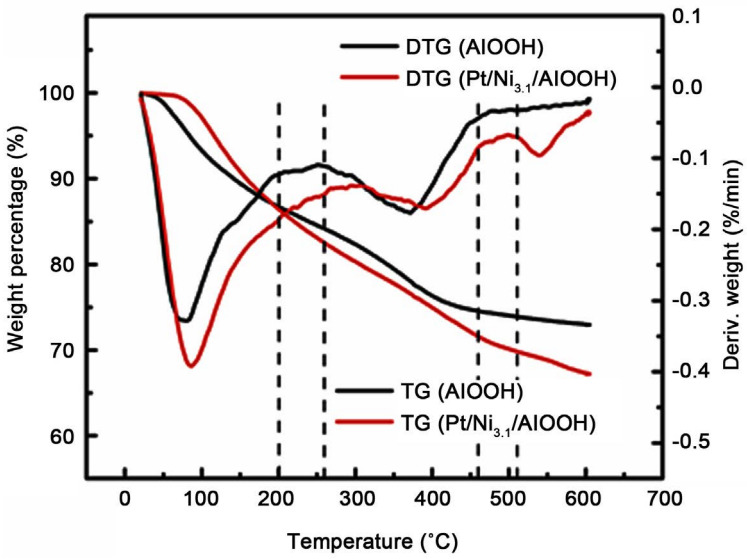

Figure 6. The curve of Thermo-gravimetric analysis over a-AlOOH and $Pt_{1.15}/Ni_{3.1}$/a-AlOOH samples.

thermal decomposed to form the third weightlessness peak. In summary, the surface of the catalyst doped with Ni had two different hydroxyl groups (Al-OH and Ni-OH), which enriched the surface active hydroxyl groups of the catalyst.

Figure 7 shows the XPS characterization of $Pt_{1.2}$/a-AlOOH and $Pt_{1.15}/Ni_{3.1}$/a-AlOOH to investigate the chemical valence states of Pt, O and Ni on the surface of the catalyst, and **Table 2** concludes the obtained data. The deconvoluted O1s signal of $Pt_{1.2}$/a-AlOOH presents three peaks at 530.4 - 530.8, 531.5 - 531.8 and 532.9 - 533.1 eV, attributed to Al-O, Al-OH, and adsorbed water (**Figure 7(a)**), respectively. For comparison, the deconvolution of the O1s signal of $Pt_{1.15}/Ni_{3.1}$/a-AlOOH gives four peaks (**Figure 7(c)**). The values of the other three peaks are similar to those of the samples without Ni, while another one is about 532.1 eV, which is attributed to O 1s in NiOOH. This corresponds to the NiOOH crystals measured in XRD. In addition, the binding energy of oxygen Al-O in the lattice of $Pt_{1.15}/Ni_{3.1}$/a-AlOOH catalyst was shifted by 0.4 eV relative to $Pt_{1.2}$/a-AlOOH to the lower energy level, which may be due to the fact that NiOOH acts as an electron donor to transfer electrons to the carrier and Pt particles. By comparing the proportions of several kinds of oxygen, the percentage of lattice oxygen (Al-O) decreased from 41.5% to 18.5% after the addition of Ni, and the surface hydroxyl (−OH) increased from 36.4% to 72.8%, indicating that the NiOOH formed after the addition of Ni, increasing the surface hydroxyl content of the catalyst.

It can be seen from **Figure 7(b)** and **Figure 7(d)** that Pt can be divided into three valence states: P^0, Pt^{2+} and Pt^{4+}. Its peak binding energy is mainly about 314.5 - 314.6 eV, 316.5 - 317.3 eV and 317.9 - 318.7 eV. The results are summarized in **Table 2**. According to **Table 2**, the value of $Pt^0/(Pt^{0+} + Pt^{2+} + Pt^{4+})$ in $Pt_{1.15}/Ni_{3.1}$/a-AlOOH catalyst was 45.3%, while that in $Pt_{1.2}$/a-AlOOH was 27.2%. This may be because the addition of Ni makes it easier to reduce Pt. According

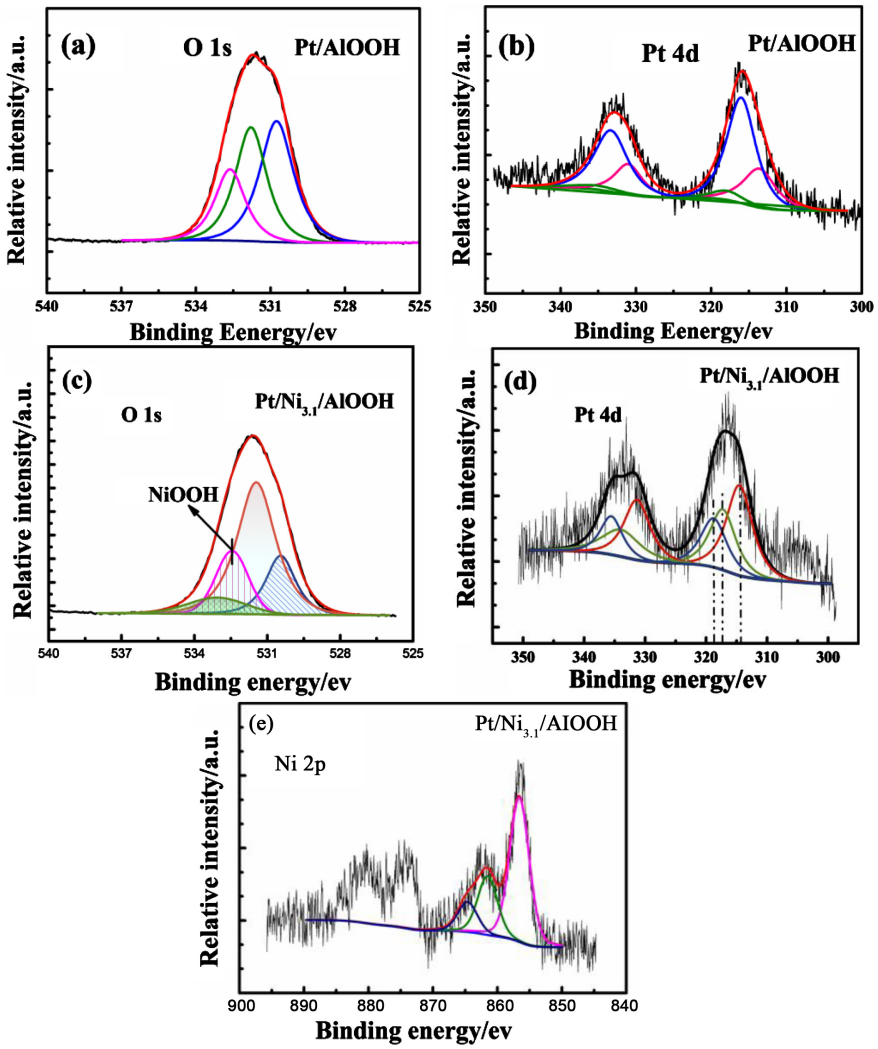

Figure 7. O 1s and Pt 4d spectra of $Pt_{1.2}$/a-AlOOH by XPS: (a) (b) O 1s and Pt 4d spectra of $Pt_{1.15}/Ni_{3.1}$/a-AlOOH by XPS: (c) (d) Ni 2p spectra of $Pt_{1.15}/Ni_{3.1}$/a-AlOOH by XPS: (e).

Table 2. characterization table of $Pt_{1.2}$/a-AlOOH and $Pt_{1.15}/Ni_{3.1}$/a-AlOOH Catalysts by XPS.

Catalysts	Binding energy/eV	Binding energy/eV	I_{OH}/I_{Total}/ %
	Pt $4d_{5/2}$/%	Al-OH, -OH, H-OH/%	
$Pt_{1.2}$/a-AlOOH	314.6 (27.2), 316.5 (66.4), 317.9 (6.4)	530.8 (41.5), 531.8 (36.4), 532.9 (22.1)	36.4
$Pt_{1.15}/Ni_{3.1}$/a-AlOOH	314.5 (45.3), 317.3 (30.3), 318.7 (24.4)	530.45 (18.5), 531.5 (53.4), 532.4 (19.4), 533.1 (8.7)	72.8

to our previous discussion, Pt^0 plays an important role in the catalytic oxidation of HCHO. It is worth noting that the binding energy of Pt^0 valence state turns to low energy level, while the binding energy of Pt^{2+} and Pt^{4+} turns to high energy level, which may be caused by the interaction between NiOOH, Pt and carrier. As the percentage of Pt^0 state in Pt particles increases, Pt particles transfer elec-

trons to nearby oxygen atoms to activate or promote the activation of adsorbed oxygen, thus improving the catalytic oxidation performance of the catalyst. In the Ni 2p spectra (**Figure 7(e)**), three peaks at 856.6 eV, 861.5 eV and 864.6 eV can be seen, which correspond to the typical NiOOH [40]. This is consistent with the characterization of XRD. Combined with the XPS analysis of O, it can be seen that the added nickel generates NiOOH, thus providing more surface hydroxyl and more adsorption sites for HCHO.

4. Conclusion

In this work, Pt/Nix/a-AlOOH catalysts were developed to promote the catalytic performance of HCHO oxidation at room temperature. The $Pt_{1.15}/Ni_{3.1}$/a-AlOOH catalyst showed the best catalytic performance at the room temperature 25˚C with CO_2 conversion of 88% and HCHO was completely oxidized at 40˚C. Characterization by XRD, TG and XPS indicated that Ni existed in the catalyst in the form of NiOOH. In addition, two different hydroxyl groups appeared in O 1s orbital, one was Al-OH and the other was Ni-OH, so the hydroxyl content of the catalyst was increased from 36.4% to 72.8%. Moreover, after loading Ni, the content of Pt^0 increased from 27.5% to 45%, which can promote the activation of O_2 near Pt particles, therefore improving the oxidation of HCHO on the catalyst. This work shows the effect of Ni loading on the surface hydroxyls of the supports on the HCHO removal performance, offering a new way of thinking for the design of the structured catalysts with high-performance for indoor air purification.

Acknowledgements

This work was financially supported by the Natural Science Foundation of Shanghai (Grant No. 16ZR1408200) and Fundamental Research Funds for the Central Universities (Grant No. 222201817013).

Conflicts of Interest

The authors declare no conflicts of interest regarding the publication of this paper.

References

[1] Nie, L.H., Yu, J.G., Jaroniec, M. and Tao, F. (2016) Room-Temperature Catalytic Oxidation of Formaldehyde on Catalysts. *Catalysis Science & Technology*, **6**, 3649-3669. https://doi.org/10.1039/C6CY00062B

[2] Jiang, C.J., Li, D.D., Zhang, P.Y., Li, J.G., Wang, J. and Yu, J.G. (2017) Formaldehyde and Volatile Organic Compound (VOC) Emissions from Particleboard: Identification of Odorous Compounds and Effects of Heat Treatment. *Building and Environment*, **117**, 118-126. https://doi.org/10.1016/j.buildenv.2017.03.004

[3] Salthammer, T., Mentese, S. and Marutzky, R. (2010) Formaldehyde in the Indoor Environment. *Chemical Reviews*, **110**, 2536-2572. https://doi.org/10.1021/cr800399g

[4] Sun, D., Le, Y., Jiang, C.J. and Cheng, B. (2018) Ultrathin Bi_2WO_6 Nanosheet Decorated with Pt Nanoparticles for Efficient Formaldehyde Removal at Room Temperature. *Applied Surface Science*, **441**, 429-437. https://doi.org/10.1016/j.apsusc.2018.02.001

[5] Wang, J.L., Zhang, P.Y., Li, J.G., Jiang, C.J., Yunus, R. and Kim, J. (2015) Room-Temperature Oxidation of Formaldehyde by Layered Manganese Oxide: Effect of Water. *Environmental science & technology*, **49**, 12372-12379. https://doi.org/10.1021/acs.est.5b02085

[6] Zhang, C.B., Liu, F.D., Zhai, Y.P., Ariga, H., Yi, N., Liu, Y.C., Asakura, K., Flytzani-Stephanopoulos, M. and He, H. (2012) Alkali-Metal-Promoted Pt/TiO_2 Opens a More Efficient Pathway to Formaldehyde Oxidation at Ambient Temperatures. *Angewandte Chemie*, **51**, 9628-9632. https://doi.org/10.1002/anie.201202034

[7] Huang, H. and Leung, D.Y.C. (2011) Complete Oxidation of Formaldehyde at Room Temperature Using TiO_2 Supported Metallic Pd Nanoparticles. *ACS Catalysis*, **1**, 348-354. https://doi.org/10.1021/cs200023p

[8] Yan, Z.X., Xu, Z.H., Yu, J.G. and Jaroniec, M. (2015) Highly Active Mesoporous Ferrihydrite Supported Pt Catalyst for Formaldehyde Removal at Room Temperature. *Environmental Science & Technology*, **49**, 6637-6644. https://doi.org/10.1021/acs.est.5b00532

[9] Tang, X.F., Chen, J.L., Huang, X.M., Xu, Y.D. and Shen, W.J. (2008) Pt/MnO_x-CeO_2 Catalysts for the Complete Oxidation of Formaldehyde at Ambient Temperature. *Applied Catalysis B*: *Environmental*, **81**, 115-121. https://doi.org/10.1016/j.apcatb.2007.12.007

[10] Zhang, C.B., Li, Y.B., Wang, Y.F. and He, H. (2014) Sodium-Promoted Pd/TiO_2 for Catalytic Oxidation of Formaldehyde at Ambient Temperature. *Environmental Science & Technology*, **48**, 5816-5822. https://doi.org/10.1021/es4056627

[11] Huang, H.B., Ye, X.G., Huang, H.L., Zhang, L. and Leung, D.Y.C. (2013) Mechanistic Study on Formaldehyde Removal over Pd/TiO_2 Catalysts: Oxygen Transfer and Role of Water Vapor. *Chemical Engineering Journal*, **230**, 73-79. https://doi.org/10.1016/j.cej.2013.06.035

[12] Yang, T.F., Huo, Y., Liu, Y., Rui, Z.B. and Ji, H. (2017) Efficient Formaldehyde Oxidation over Nickel Hydroxide Promoted Pt/γ-Al_2O_3 with a Low Pt Content. *Applied Catalysis B*: *Environmental*, **200**, 543-551. https://doi.org/10.1016/j.apcatb.2016.07.041

[13] Wang, R.H. and Li, J.H. (2009) OMS-2 Catalysts for Formaldehyde Oxidation: Effects of Ce and Pt on Structure and Performance of the Catalysts. *Catalysis Letters*, **131**, 500-505. https://doi.org/10.1007/s10562-009-9939-5

[14] Shi, Y.Y., Qiao, Z.W., Liu, Z.L. and Zuo, J.L. (2019) Cerium Doped Pt/TiO_2 for Catalytic Oxidation of Low Concentration Formaldehyde at Room Temperature. *Catalysis Letters*, **149**, 1319-1325. https://doi.org/10.1007/s10562-019-02684-z

[15] Jia, M.L., Shen, Y.N., Li, C.Y., Bao, Z. and Sheng, S.S. (2005) Effect of Supports on the Gold Catalyst Activity for Catalytic Combustion of CO and HCHO. *Catalysis Letters*, **99**, 235-239. https://doi.org/10.1007/s10562-005-2129-1

[16] Yusuf, A., Snape, C., He, J., Xu, H.H., Liu, C.J., Zhao, M., Chen, G.Z., Tang, B., Wang, C.J, Wang, J.W. and Behera, A.N. (2017) Advances on Transition Metal Oxides Catalysts for Formaldehyde Oxidation: A Review. *Catalysis Reviews*, **18**, 1-45. https://doi.org/10.1080/01614940.2017.1342476

[17] Wang, J.L., Li, J.G., Jiang, C.J., Zhou, P., Zhang, P.Y. and Yu, J.G. (2017) The Effect of Manganese Vacancy in Birnessite-Type MnO_2 on Room-Temperature Oxidation

of Formaldehyde in Air. *Applied Catalysis B*: *Environmental*, **204**,147-155. https://doi.org/10.1016/j.apcatb.2016.11.036

[18] Rong, S.P., Zhang, P.Y., Wang, J.L., Liu, F., Yang, Y.J., Yang, G.L. and Liu, S. (2016) Ultrathin Manganese Dioxide Nanosheets for Formaldehyde Removal and Regeneration Performance. *Chemical Engineering Journal*, **306**, 1172-1179. https://doi.org/10.1016/j.cej.2016.08.059

[19] Zheng, Y.L., Wang, W.Z., Jiang, D. and Zhang, L. (2016) Amorphous MnO_x Modified Co_3O_4 for Formaldehyde Oxidation: Improved Low-Temperature Catalytic and Photothermocatalytic Activity. *Chemical Engineering Journal*, **284**, 21-27. https://doi.org/10.1016/j.cej.2015.08.137

[20] Bai, B.Y., Arandiyan, H. and Li, J. (2013) Comparison of the Performance for Oxidation of Formaldehyde on Nano-Co_3O_4, 2D-Co_3O_4, and 3D-Co_3O_4 Catalysts. *Applied Catalysis B*: *Environmental*, **142**-**143**, 677-683. https://doi.org/10.1016/j.apcatb.2013.05.056

[21] Zeng, L., Song, W.L., Li, M.H., Zeng, D.W. and Xie, C.S. (2014) Catalytic Oxidation of Formaldehyde on Surface of H-TiO_2/H-C-TiO_2 without Light Illumination at Room Temperature. *Applied Catalysis B*: *Environmental*, **147**, 490-498. https://doi.org/10.1016/j.apcatb.2013.09.013

[22] Park, S.M., Jeon, S.W. and Kim, S.H. (2014) Formaldehyde Oxidation Over Manganese-Cerium-Aluminum Mixed Oxides Supported on Cordierite Monoliths at Low Temperatures. *Catalysis Letters*, **144**,756-766. https://doi.org/10.1007/s10562-014-1207-7

[23] Huang, Q., Lu, Y.Y., Si, H., Yang, B., Tao, T., Zhao, Y.X. and Chen, M. (2018) Study of Complete Oxidation of Formaldehyde over MnOx-CeO_2 Mixed Oxide Catalysts at Ambient Temperature. *Catalysis Letters*, **148**, 2880-2890. https://doi.org/10.1007/s10562-018-2479-0

[24] He, M., Ji, J., Liu, B.Y. and Huang, H. (2019) Reduced TiO_2 with Tunable Oxygen Vacancies for Catalytic Oxidation of Formaldehyde at Room Temperature. *Applied Surface Science*, **473**, 934-942. https://doi.org/10.1016/j.apsusc.2018.12.212

[25] Cui, W.Y., Xue, D., Yuan, X.L., Zheng, B., Jia, M.J. and Zhang, W.X. (2017) Acid-Treated TiO_2 Nanobelt Supported Platinum Nanoparticles for the Catalytic Oxidation of Formaldehyde at Ambient Conditions. *Applied Surface Science*, **411**, 105-112. https://doi.org/10.1016/j.apsusc.2017.03.169

[26] Chen, B.B., Zhu, X.B., Crocker, M., Wang, Y. and Shi, C. (2013) Complete Oxidation of Formaldehyde at Ambient Temperature over γ-Al_2O_3 Supported Au Catalyst. *Catalysis Communications*, **42**, 93-97. https://doi.org/10.1016/j.catcom.2013.08.008

[27] Yan, Z.X., Xu, Z.H., Yu, J.G. and Jaroniec, M. (2016) Enhanced Formaldehyde Oxidation on CeO_2/AlOOH-Supported Pt Catalyst at Room Temperature. *Applied Catalysis B*: *Environmental*, **199**, 458-465. https://doi.org/10.1016/j.apcatb.2016.06.052

[28] Chen, F., Wang, F., Li, Q., Cao, C.Y., Zhang, X., Ma, H. and Guo, Y. (2017) Effect of Support (Degussa P25 TiO_2, Anatase TiO_2, γ-Al_2O_3, and AlOOH) of Pt-Based Catalysts on the Formaldehyde Oxidation at Room Temperature. *Catalysis Communications*, **99**, 39-42. https://doi.org/10.1016/j.catcom.2017.05.019

[29] Liu, B.C., Liu, Y., Li, C.Y., Hu, W.T., Jing, P., Wang, Q. and Zhang, J. (2012) Three-Dimensionally Ordered Macroporous Au/CeO_2-Co_3O_4 Catalysts with Nanoporous Walls for Enhanced Catalytic Oxidation of Formaldehyde. *Applied Catalysis B*: *Environmental*, **127**, 47-58. https://doi.org/10.1016/j.apcatb.2012.08.005

[30] Chen, B.B., Shi, C., Crocker, M., Wang, Y. and Zhu, A. (2013) Catalytic Removal of

Formaldehyde at Room Temperature over Supported Gold Catalysts. *Applied Catalysis B*: *Environmental*, **132**-**133**, 245-255. https://doi.org/10.1016/j.apcatb.2012.11.028

[31] Li, H.F., Zhang, N., Peng, C., Luo, M.F. and Lu, J.Q. (2011) High Surface Area Au/CeO_2 Catalysts for Low Temperature Formaldehyde Oxidation. *Applied Catalysis B*: *Environmental*, **110**, 279-285. https://doi.org/10.1016/j.apcatb.2011.09.013

[32] Ou, C.C., Chen, C.H., Chan, T.S., Chen, C.S. and Cheng, S. (2019) Influence of Pretreatment on the Catalytic Performance of Ag/CeO_2 for Formaldehyde Removal at Low Temperature. *Journal of Catalysis*, **380**, 43-54. https://doi.org/10.1016/j.jcat.2019.09.028

[33] Chen, Y., He, J.H., Tian, H., Wang, D.H. and Yang, Q.W. (2014) Enhanced Formaldehyde Oxidation on Pt/MnO_2 Catalysts Modifiedwith Alkali Metal Salts. *Journal of Colloid and Interface Science*, **428**, 1-7. https://doi.org/10.1016/j.jcis.2014.04.028

[34] Sun, X.C., Lin, J., Guan, H.L., Li, L., Sun, L., Wang, Y.H., Miao, S., Su, Y. and Wang, X.D. (2018) Complete Oxidation of Formaldehyde over TiO_2 Supported Subnanometer Rh Catalyst at Ambient Temperature. *Applied Catalysis B*: *Environmental*, **226**, 575-584. https://doi.org/10.1016/j.apcatb.2018.01.011

[35] Yan, Z.X., Xu, Z.H., Yu, J.G. and Jaroniec, M. (2017) Effect of Microstructure and Surface Hydroxyls on the Catalytic Activity of Au/AlOOH for Formaldehyde Removal at Room Temperature. *Journal of Colloid and Interface Science*, **501**, 164-174. https://doi.org/10.1016/j.jcis.2017.04.050

[36] Zhang, Q., Wang, T.Y., Fu, W.Z. and Duan, X.Z. (2018) Facet-Dependent Performance of Hydroxylated Anodic Boehmite for Catalyzing Gaseous Formaldehyde Oxidation. *Catalysis Letters*, **148**, 1904-1913. https://doi.org/10.1007/s10562-018-2400-x

[37] Zhang, Q., Jiang, Z.R., Sun, D.M., Han, D.Y. and Zhu, Z.B. (2012) Effect of Crystalline State of Anodized Porous Al_2O_3/Al as Supports by Hydration. *Journal of Inorganic Materials*, **27**, 693-698. https://doi.org/10.3724/SP.J.1077.2012.11552

[38] Zhang, Q., Sun, S.B., Wang, T.Y., Liu, F., Yang, J.H. and Cheng, A. (2018) Fe Promoted Structured Pt/Fe_x/a-AlOOH Catalyst for Room Temperature Oxidation of Low Concentration HCHO. *Chemical Engineering Processing*, **132**, 169-174. https://doi.org/10.1016/j.cep.2018.07.003

[39] Zhao, G.B., Zhang, Q., Cheng, F. and Wang, T.Y. (2018) Effects of Sodium-Modified Pt/AlOOH Catalyst on Activity of Formaldehyde Oxidation. *Journal Chemical Industry*, **69**, 4722-4727.

[40] Biesinger, M.C., Payne, B.P., Grosvenor, A.P., Lau, L.W.M., Gerson, A.R. and Smart, R.S.C. (2011) Resolving Surface Chemical States in XPS Analysis of First Row Transition Metals, Oxides and Hydroxides: Cr, Mn, Fe, Co and Ni. *Applied Surface Science*, **257**, 2717-2730. https://doi.org/10.1016/j.apsusc.2010.10.051